*Inorg. Chem.* **2005**, *44*, 431−442

# "Venetian Blinds" Mechanism of Solvation/Desolvation in Palladium(II) Wheel-and-Axle Organic−Inorganic Diols

**Alessia Bacchi,* Elsa Bosetti, Mauro Carcelli, Paolo Pelagatti, Dominga Rogolino, and Giancarlo Pelizzi**

*Dipartimento di Chimica Generale ed Inorganica, Chimica Analitica, Chimica Fisica, University of Parma, Parco Area delle Scienze, 17A, 43100 Parma, Italy*

Received August 11, 2004

A family of organic−inorganic wheel-and-axle diols ($Pd(LOH)_2Cl_2$, $Pd(LOH)_2(CH_3)Cl$, $Pd(LOH)_2(CH_3COO)_2$, LOH = α-(4-pyridyl)benzhydrol) and several corresponding solvates are synthesized and characterized by single-crystal X-ray diffraction analysis. Their structures are compared to investigate the factors governing the modes of solid state association, the propensity to clathration, and the structural basis of guest inclusion. In all the complexes, the palladium coordination is a slightly distorted square. The LOH ligands coordinate $Pd^{2+}$ by means of the 4-pyridyl ring. In the chloride complexes solvation occurs with a 1:2 host/guest ratio by hydrogen bonding between the terminal −OH groups of the complex diol and one acceptor atom on the guest, and it is further assisted by guest stacking between host aryl rings. All solvates are organized in layers with practically invariant metrics, while the layers may be assembled in different arrangements. The structures of the nonsolvate compounds are related to the metrics of the solvate forms by rotation of the complex molecules within the layer plane. In all cases the nonsolvates are completely converted into the corresponding crystalline solvate forms by exposure to the vapor of the guest, and conversely they are quantitatively recovered from the solvate upon removal of the guest by mild conditions. On the basis of the structural data, it is proposed that the solvation/desolvation process proceeds by a concerted rotation of the complex molecules in the layer plane. The structural analysis of $Pd(LOH)_2(CH_3COO)_2$ and of its tetrahydrofuran monosolvate form suggests that the first step of the solid/gas solvation process may imply the clathration of 1 mol of guest between the aryl rings, which successively triggers the collective reorientation of the host molecules.

## Introduction

The rational design of new porous solids based on the combination of soft supramolecular interactions and coordination bond is attracting the interest of many researchers in the field of crystal engineering, in view of the potential utilization of these materials for heterogeneous catalysis, solid-state "green" chemistry, and sensor applications.[1] The "wheel-and-axle" diols have been extensively studied for their versatility as hosts for a variety of solvent guests.[2] Wheel-and-axle diols are organic molecules with a long, usually linear axis with large, rigid substituents at both ends. Their propensity to include small molecules in the crystal lattice derives from the combination of the hydrogen bond donor capability of the OH groups with the steric bulkiness of the terminal diaryl groups.[3] The prototypical system is $HO-C(Ar)_2-L-(Ar)_2C-OH$, where L is a suitable rigid spacer (e.g. fused rings or triple bonds). Our purpose is to use a metal to build in an innovative way the L spacer, thus obtaining organic−inorganic wheel-and-axle diols.[4] With this aim, we have synthesized crystalline compounds by coor-

* Author to whom correspondence should be addressed. E-mail: alessia.bacchi@unipr.it.

(1) (a) Yoo, S.-K.; Ryu, J. Y.; Lee, J. Y.; Kim, C.; Kim, S.-J.; Kim, Y. *J. Chem. Soc., Dalton Trans.* **2003**, 1454. (b) Kaupp, G. *Cryst. Eng. Commun.* **2003**, *5*, 117. (c) Reinbold, J.; Buhlmann, K.; Cammann, K.; Wierig, A.; Wimmer, C.; Weber, E. *Sens. Actuators, B* **1994**, *18*, 77.

(2) (a) Weber, E.; Skobridis, K.; Wierig, A.; Nassimbeni, L. R.; Johnson, L. *J. Chem. Soc., Perkin Trans. 2* **1992**, 2123. (b) Johnson, L.; Nassimbeni, L. R.; Weber, E.; Skobridis, K. *J. Chem. Soc., Perkin Trans. 2* **1992**, 2131. (c) Caira, M. R.; Jacobs, A.; Nassimbeni, L. R.; Toda, F. *Cryst. Eng. Commun*. **2003**, *5*, 150−153. (d) Caira, M. R.; Nassimbeni, L. R.; Toda, F.; Vujovic, D. *J. Chem. Soc., Perkin Trans. 2* **2001**, 2119−2124. (e) Csoregh, I.; Brehmer, T., Nitsche, S. I.; Seichter, W.; Weber, E. *J. Inclusion Phenom. Macrocyclic Chem.* **2003**, *47*, 113−121.

(3) Toda, F. *Comp. Supramol. Chem.* **1996**, *6*, 465−516.

10.1021/ic048896m CCC: $30.25 
Published on Web 12/29/2004

**Chart 1.** Hybrid Organic−Inorganic Prototypal Diol

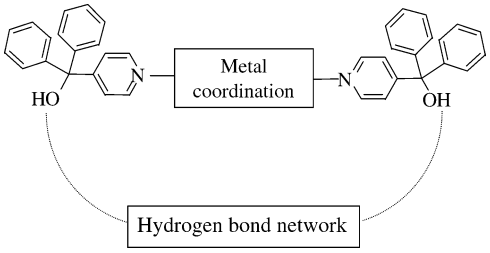


dinating α-(4-pyridyl)benzhydrol (LOH) to transition metals with various geometric and chemical properties; the final structural and clathrating properties will depend on the metal coordination number, geometry, and configuration, on the steric and supramolecular characteristics of the counteranions, and on the hydrogen bond network involving the carbinol −OH groups (Chart 1). It is also worth of note that the use of a metal allows one to obtain molecules with a long principal axle that are interesting to widen the available network space,[5] without the laborious procedures of the organic synthesis. Metals with propensity to low coordination numbers are the natural initial choice to design networks with low steric hindrance in the middle of the molecular axle. We have recently presented the first results concerning the rationalization of the supramolecular organization of a series of silver compounds.[6] In this work we report and compare the crystal organization of a family of palladium complexes, $Pd(LOH)_2Cl_2$, $Pd(LOH)_2(CH_3)Cl$, $Pd(LOH)_2(CH_3COO)_2$, and several related solvates, to investigate the factors governing the modes of solid-state association, the propensity to clathration, and the structural bases of guest inclusion. We also explore the possibility to convert between the solvate and the nonsolvate forms via solid/gas processes, and we propose a mechanism for the observed reversible solvation/desolvation with retention of crystallinity. The response of molecular conformation to clathration is also analyzed.

## Experimental Section

**Synthesis.** $[Pd(PhCN)_2Cl_2]$[7] and [Pd(COD)MeCl][8] were synthesized by following literature methods. The ligand α-(4-pyridyl)-benzhydrol (Aldrich, 75%) was recrystallized from boiling $CH_2Cl_2$. Proton NMR spectra were recorded at 27 °C on a Bruker 300 FT spectrophotometer by using $SiMe_4$ as internal standard, while IR spectra were obtained with a Nicolet 5PCFT-IR spectrophotometer in the 4000−400 $cm^{-1}$ range, using KBr disks. Elemental analyses were performed by using a Carlo Erba model EA 1108 apparatus.

**$[Pd(LOH)_2Cl_2]$ (1).** A $CH_2Cl_2$ solution (40 mL) of LOH (0.074 g, $2.84 \times 10^{-4}$ mol) was slowly added to a $CH_2Cl_2$ solution (10 mL) of $Pd(PhCN)_2Cl_2$ (0.040 g, $1.42 \times 10^{-4}$ mol). The mixture was stirred magnetically at room temperature for 3 h; a yellow powder was filtered off, washed with diethyl ether, and dried in vacuo. The product was recrystallized from 1,4-dioxane at room temperature, and yellow crystals were obtained. Yield: 73%. Mp: 300 °C (dec). Anal. Calcd for $C_{36}H_{30}Cl_2N_2O_2Pd$ ($M_r$ = 699.94): C, 61.77; H, 4.31; N, 4.00. Found: C, 61.82; H, 4.96; N, 3.52. IR (KBr, $cm^{-1}$): $\nu$(O−H) 3403 (m), $\nu$(C−H) 3056, 2919, 2850 (w). $^1$H NMR ($CDCl_3$, 25 °C, ppm): $\delta$ 8.73 (d, $J_{H,H}$ = 6.67 Hz, 4H, C(4)−H, C(5)−H), 7.36−7.19 (m, 24H, Ar + C(3)−H + C(6)−H). $^1$H NMR ($(CD_3)_2SO$, 25 °C, ppm): $\delta$ 8.66 (d, 4H, $J_{H,H}$ = 5.53 Hz, C(4)−H, C(5)−H), 7.46−7.19 (m, 24H, Ar + C(3)−H + C(6)−H), 6.93 (s, 2H, −OH, $D_2O$ exchangeable). $^1$H NMR ($(CD_3)_2CO$, 25 °C, ppm): $\delta$ 8.75 (d, $J_{H,H}$ = 6.82 Hz, 4H, C(4)−H, C(5)−H), 7.49−7.31 (m, 24H, Ar + C(3)−H + C(6)−H), 3.57 (s, 2H, −OH, $D_2O$ exchangeable).

**$[Pd(LOH)_2Cl_2]\cdot 2(CH_3)_2CO$ (2).** A 100 mg amount of **1** was dissolved in acetone, and the solution was left at room temperature for some days. Yellow crystals of **2** were filtered off (yield 92%; mp 300 °C (dec)). Compound **2** was also obtained by exposing 100 mg of **1** to vapors of acetone for 5 days. The quantitative formation of **2** was assessed by comparing the X-ray powder diffraction pattern of the crystalline product with the spectrum calculated on the basis of the single-crystal structure. The experimental pattern contained also some weak peaks belonging to crystalline LOH, quantified in a few percent impurity. Anal. Calcd for $C_{42}H_{42}Cl_2N_2O_4Pd$ ($M_r$ = 816.12): C, 61.83; H, 5.14; N, 3.42. Found: C, 61.70; H, 5.13; N, 3.50. IR (KBr, $cm^{-1}$): $\nu$(O−H) 3362 (m), $\nu$(C=O) 1688 (s). $^1$H NMR ($CDCl_3$, 25 °C, ppm): $\delta$ 8.72 (d, $J_{H,H}$ = 6.62 Hz, 4H, C(4)−H, C(5)−H), 7.37−7.18 (m, 24H, Ar + C(3)−H + C(6)), 2.16 (s, 12H, $(CH_3)_2CO$). Thermogravimetric data: experimental mass loss, 13.67%; calcd for two acetone molecules, 14.22%.

**$[Pd(LOH)_2Cl_2]\cdot 2DMSO$ (3).** A sample of $[Pd(LOH)_2Cl_2]$ was recrystallized from DMSO, the solution was left at room temperature for some days, and yellow crystals were filtered off. Yield: 42%. Mp: 300 °C (dec). Anal. Calcd for $C_{40}H_{42}Cl_2N_2O_2PdS_2$ ($M_r$ = 856.12): C, 56.11; H, 4.90; N, 3.27; S, 7.48. Found: C, 56.03; H, 5.18; N, 3.54; S, 7.85. IR (KBr, $cm^{-1}$): $\nu$(O−H) 3100 (m), $\nu$(C−H) 3102, $\nu$(S=O) 1049 (s). $^1$H NMR ($CDCl_3$, 25 °C, ppm): $\delta$ 8.70 (d, $J_{H,H}$ = 6.72 Hz, 4H, C(4)−H, C(5)−H), 7.35−7.18 (m, 24H, Ar + C(3)−H + C(6)−H), 2.57 (s, 12H, $CH_3$ (DMSO)).

**$[Pd(LOH)_2Cl_2]\cdot 2DMF$ (4).** A 100 mg amount of **1** was dissolved in DMF, and the solution was left at room temperature for some days. Yellow crystals of **4** were filtered off. Yield: 73%. Mp: 300 °C (dec). Anal. Calcd for $C_{42}H_{42}Cl_2N_4O_4Pd$ ($M_r$ = 845.78): C, 59.64; H, 5.20; N, 6.62. Found: C, 59.20; H, 5.24; N, 6.69. IR (KBr, $cm^{-1}$): $\nu$(O−H) 3279 (m), $\nu$(C(Ar)−H) 3102, $\nu$(C−H) 2927, 2874, $\nu$(C=O) 1660 (s). $^1$H NMR ($CDCl_3$, 25 °C, ppm): $\delta$ 8.72 (d, $J_{H,H}$ = 6.63 Hz, 4H, C(4)−H, C(5)−H), 7.97 (s, 2H, −COH (DMF)), 7.36−7.18 (m, 24H, Ar + C(3)−H + C(6)−H), 2.94 (s, 6H, $CH_3$ (DMF)), 2.86 (s, 6H, $-CH_3$ (DMF)). Thermogravimetric data: experimental mass loss, 17.01%; calcd for two DMF molecules, 17.28%.

**$[Pd(LOH)_2Cl_2]\cdot 2THF$ (5).** A THF solution (40 mL) of LOH (0.074 g, $2.84 \times 10^{-4}$ mol) was slowly added to a THF solution (10 mL) of $Pd(PhCN)_2Cl_2$ (0.040 g, $1.42 \times 10^{-4}$ mol). The mixture was stirred at room temperature for 3 h, and then the solution was concentrated and diethyl ether was added (40 mL). After 1 day at −18 °C, yellow crystals were formed. Yield: 84%. Mp: 300 °C (dec). Anal. Calcd for $C_{44}H_{46}Cl_2N_2O_4Pd$ ($M_r$ = 843.90): C, 62.62; H, 5.45; N, 3.33. Found: C, 62.98; H, 5.18; N, 3.54. IR (KBr, $cm^{-1}$): $\nu$(O−H) 3284 (m), $\nu$(C−H) 2879 (w). $^1$H NMR ($CDCl_3$, 25 °C, ppm): $\delta$ 8.71 (d, $J_{H,H}$ = 6.67 Hz, 4H, C(4)−H, C(5)−H),

(4) As far as we know, the only precedent can be found in the following: Sembirin, S. B.; Colbran, S. B.; Bishop, R.; Craig, D. C.; Rae, A. D. *Inorg. Chim. Acta* **1995**, *228*, 109−117.
(5) Weber, E.; Hens, Th.; Brehmer, Th; Csoregh, I. *J. Chem Soc., Perkin Trans. 2* **2000**, 235−241.
(6) (a) Bacchi, A.; Bosetti, E.; Carcelli, M.; Pelagatti, P.; Rogolino, D. *Eur. J. Inorg. Chem.* **2004**, 1985−1991. (b) Bacchi, A.; Bosetti, E.; Carcelli, M.; Pelagatti, P.; Rogolino D. *Cryst. Eng. Commun.* **2004**, *6*, 177−183.
(7) Anderson, G. K.; Lin, M. *Inorg. Synth.* **1990**, *28*, 61−62.
(8) Rulke, R. E.; Ernsting, J. M.; Spek, A. L.; Elsevier, C. J.; van Leeuwen, P. W. N. M.; Vrieze, K. *Inorg. Chem.* **1993**, *32*, 5769−5778.

**Table 1.** Crystal Data for Compounds **1**−**10**

| | **1** | **2** | **3** | **4** | **5** |
|---|---|---|---|---|---|
| formula | $C_{36}H_{30}Cl_2N_2O_2Pd$ | $C_{42}H_{42}Cl_2N_2O_4Pd$ | $C_{40}H_{42}Cl_2N_2O_4PdS_2$ | $C_{42}H_{42}Cl_2N_4O_4Pd$ | $C_{44}H_{46}Cl_2N_2O_4Pd$ |
| fw | 699.92 | 816.08 | 856.18 | 844.10 | 844.13 |
| cryst system | monoclinic | monoclinic | monoclinic | monoclinic | triclinic |
| space group | $P2_1/n$ | $P2_1/n$ | $P2_1/n$ | $P2_1/c$ | $P\bar{1}$ |
| $Z$ | 4 | 2 | 2 | 2 | 1 |
| $a$/Å | 10.736(2) | 7.2997(9) | 7.6906(3) | 7.191(8) | 7.9754(7) |
| $b$/Å | 17.410(2) | 18.591(2) | 18.5017(8) | 15.06(2) | 11.220(1) |
| $c$/Å | 16.933(2) | 14.631(2) | 14.5046(5) | 18.84(2) | 11.543(1) |
| α/deg | | | | | 100.534(2) |
| $\beta$/deg | 95.584(2) | 103.959(2) | 106.166(2) | 88.17(2) | 96.889(2) |
| $\gamma$/deg | | | | | 98.944(2) |
| $V$/Å$^3$ | 3150.0(8) | 1926.9(4) | 1982.2(1) | 2039(4) | 991.4(1) |
| $\rho$/Mg m$^{-3}$ | 1.476 | 1.407 | 1.434 | 1.375 | 1.414 |
| unique reflcns | 4523 | 4787 | 5123 | 4774 | 5280 |
| obsd reflcns [$I > 2\sigma(I)$] | 2977 | 4023 | 4115 | 3997 | 5009 |
| params | 508 | 237 | 294 | 245 | 301 |
| R1 [$I > 2\sigma(I)$] | 0.0365 | 0.0619 | 0.0307 | 0.1202 | 0.0250 |
| wR2 [$I > 2\sigma(I)$] | 0.0706 | 0.1559 | 0.0881 | 0.3252 | 0.0684 |
| R1 (all data) | 0.0701 | 0.0717 | 0.0411 | 0.1344 | 0.0275 |
| wR2 (all data) | 0.0784 | 0.1588 | 0.0933 | 0.3313 | 0.071 |

| | **6** | **7** | **8** | **9** | **10** |
|---|---|---|---|---|---|
| formula | $C_{37}H_{33}ClN_2O_2Pd$ | $C_{45}H_{49}ClN_2O_4Pd$ | $C_{43}H_{45}ClN_2O_4Pd$ | $C_{44}H_{44}N_2O_7Pd$ | $C_{40}H_{36}N_2O_6Pd$ |
| fw | 679.50 | 823.71 | 795.66 | 819.21 | 747.11 |
| cryst system | monoclinic | triclinic | triclinic | triclinic | triclinic |
| space group | $P2_1/n$ | $P1$ | $P\bar{1}$ | $P1$ | $P1$ |
| $Z$ | 4 | 1 | 1 | 1 | 1 |
| $a$/Å | 10.820(4) | 8.027(3) | 7.4639(8) | 7.9303(5) | 7.569(2) |
| $b$/Å | 17.386(9) | 11.255(3) | 11.4710(8) | 11.1789(7) | 9.995(2) |
| $c$/Å | 16.85(2) | 11.550(2) | 11.7479(8) | 11.8089(7) | 12.394(3) |
| α/deg | | 100.41(3) | 101.948(1) | 84.133(1) | 89.584(4) |
| $\beta$/deg | 94.12(5) | 96.37(3) | 95.957(1) | 88.154(1) | 88.114(4) |
| $\gamma$/deg | | 98.95(4) | 96.190(1) | 77.3930(9) | 80.596(3) |
| $V$/Å$^3$ | 3162(4) | 1003.4(5) | 970.0(1) | 1016.2(1) | 924.5(4) |
| $\rho$/Mg m$^{-3}$ | 1.428 | 1.363 | 1.362 | 1.339 | 1.342 |
| unique reflcns | 6907 | 4847 | 2778 | 8250 | 2123 |
| obsd reflcns [$I > 2\sigma(I)$] | 3255 | 3065 | 2681 | 7448 | 1934 |
| params | 404 | 481 | 207 | 498 | 133 |
| R1 [$I > 2\sigma(I)$] | 0.0623 | 0.0464 | 0.0377 | 0.0315 | 0.0834 |
| wR2 [$I > 2\sigma(I)$] | 0.1325 | 0.0819 | 0.1051 | 0.0705 | 0.2107 |
| R1 (all data) | 0.1651 | 0.0936 | 0.0389 | 0.0361 | 0.0980 |
| wR2 (all data) | 0.1788 | 0.0955 | 0.1064 | 0.0729 | 0.2343 |

7.37−7.18 (m, 24H, Ar + C(3)−H + C(6)), 3.72 (m, 8H, THF), 1.82 (m, 8H, THF).

**[Pd(LOH)$_2$(CH$_3$)Cl]·2THF (7).** A THF dry solution (50 mL) of LOH (0.153 g, 5.8 × 10$^{-4}$ mol) was slowly added under $N_2$ to a THF dry solution (10 mL) of Pd(COD)MeCl (0.079 g, 2.9 × 10$^{-4}$ mol). The mixture was stirred magnetically at room temperature for 1 day, and then the solution was evaporate and diethyl ether was added (20 mL). After 1 day at −18 °C yellow crystals of **7** were formed. Yield: 76%. Mp: 54 °C (dec). Anal. Calcd for $C_{45}H_{49}ClN_2O_2Pd$ ($M_r$ = 827.21): C, 65.34; H, 5.97; N, 3.39. Found: C, 65.64; H, 5.95; N, 3.40. IR (KBr, cm$^{-1}$): $\nu$(O−H) 3289 (m), $\nu$(C−H) 2967, 2876. $^1$H NMR ($CDCl_3$, 25 °C, ppm): $\delta$ 8.75−8.69 (dd, $J_{H,H}$ = 6 Hz, 4H, C(4)−H, C(5)−H), 7.35−7.18 (br, 24H, Ar + C(3)−H + C(6)−H), 3.72−3.68 (m, 4H, THF), 3.00 (s, 2H, −OH, $D_2O$ exchangeable), 1.85−1.80 (m, 4H, THF), 0.77 (s, 3H, $CH_3$).

**[Pd(LOH)$_2$(CH$_3$)Cl] (6).** Recrystallization of **7** in $CHCl_3$ gives partial decomposition of the complex and crystals of **6**, which were characterized by single-crystal X-ray diffraction.

**[Pd(LOH)$_2$(CH$_3$)Cl]·2(CH$_3$)$_2$CO (8).** A 100 mg amount of [Pd(LOH)$_2$(CH$_3$)Cl]·2THF was recrystallized from acetone, the solution was left at room temperature for some days, and yellow crystals were filtered off. Yield: 81%. Mp: 72 °C (dec). Anal. Calcd for $C_{43}H_{45}ClN_2O_4Pd$ ($M_r$ = 795.70): C, 64.91; H, 5.70; N, 3.52. Found: C, 64.52; H, 5.33; N, 3.21. IR (KBr, cm$^{-1}$): $\nu$(O−H) 3368 (m), $\nu$(C(Ar)−H) 3054, $\nu$(C−H) 2960, 2883, $\nu$(C═O) 1694 (s). $^1$H NMR ($CDCl_3$, 25 °C, ppm): $\delta$ 8.74−8.69 (dd, $J_{H,H}$ = 6 Hz, 4H, C(4)−H, C(5)−H), 7.35−7.18 (br, 24H, Ar + C(3)−H + C(6)−H + C(21)−H + C(24) + H), 3.13 (s, 2H, OH, $D_2O$ exchangeable), 2.14 (s, 12H, $(CH_3)_2CO$), 0.77 (s, 3H, $CH_3$).

**[Pd(LOH)$_2$(OAc)$_2$]·THF (9).** A THF solution (50 mL) of LOH (0.10 g, 3.82 × 10$^{-4}$ mol) was slowly added to a THF solution (10 mL) of $Pd(OAc)_2$ (0.042 g, 1.87 × 10$^{-4}$ mol). The mixture was stirred magnetically at room temperature. After a few minutes a yellow powder was formed. The mixture was filtered, and the precipitate was washed with diethyl ether and dried in vacuo. Yield: 72%. Mp: 179 °C (dec). Anal. Calcd for $C_{44}H_{44}N_2O_7Pd$ ($M_r$ = 819.025): C, 64.52; H, 5.37; N, 3.43. Found: C, 64.26; H, 5.26; N, 3.11. IR (KBr, cm$^{-1}$): $\nu$(O−H) 3232 (m), $\nu$(C(Ar)−H) 3049 (w), $\nu$(C−H) 2973 (w). $^1$H NMR (DMSO, 25 °C, ppm): $\delta$ 8.51 (d, $J_{H,H}$ = 6.9 Hz, 4 H, C(4)−H, C(5)−H), 7.42−7.18 (br, 24H, Ar + C(3)−H + C(6)−H), 6.91 (s, 2H, −OH, $D_2O$ exchangeable), 3.61−3.58 (m, 4H, THF), 1.85−1.80 (m, 4H, THF), 1.68 (s, 6H, OAc). Thermogravimetric data: experimental mass loss (9.18%) corresponds to one THF molecule (calcd: 8.82%). X-ray-quality crystals of **9** were obtained by recrystallization from a mixture of $CHCl_3$/THF (1:1).

**[Pd(LOH)$_2$(OAc)$_2$] (10).** Single crystals of **10** were obtained by recrystallization of **9** in $CHCl_3$ and were characterized by single-

**Chart 2.** Synthesis of the Complexes **1**-**10**

| Reagents | Solvents | Product | Recrystallization solvents | Product |
|---|---|---|---|---|
| $Pd(NCPh)_2Cl_2$ + LOH | $CH_2Cl_2$ | $Pd(LOH)_2Cl_2$ (**1**) | $(CH_3)_2CO$ | $Pd(LOH)_2Cl_2.2(CH_3)_2CO$ (**2**) |
| | | | DMSO | $Pd(LOH)_2Cl_2.2$ DMSO (**3**) |
| | | | DMF | $Pd(LOH)_2Cl_2.2$ DMF (**4**) |
| | THF | $Pd(LOH)_2Cl_2.2THF$ (**5**) | | |
| $Pd(COD)(CH_3)Cl$ + LOH | THF | $Pd(LOH)_2(CH_3)Cl.2THF$ (**7**) | $CHCl_3$ | $Pd(LOH)_2(CH_3)Cl$ (**6**) |
| | | | $(CH_3)_2CO$ | $Pd(LOH)_2(CH_3)Cl.2(CH_3)_2CO$ (**8**) |
| $Pd(OAc)_2$ + LOH | THF | $Pd(LOH)_2(OAc)_2.THF$ (**9**) | $CHCl_3$ | $Pd(LOH)_2(OAc)_2$ (**10**) |

crystal X-ray diffraction. The homogeneity of the bulk was assessed by X-ray powder diffraction.

**Thermal Analyses.** Thermogravimetry (TGA) measurements were performed on a Perkin-Elmer thermogravimetrical analyzer TGA7, and differential scanning calorimetry (DSC) measurements, on a Perkin-Elmer differential scanning calorimeter DSC7 and Mettler Toledo Star system. For TGA analyses the samples were placed in open platinum pans, and for DSC the samples were placed in closed and vented aluminum pans. The TGA and DSC traces were obtained on heating the samples at 5 °C/min from 25 to 350 °C for compounds **2** and **4** and from 25 to 250 °C for compound **9**.

**Powder Diffraction.** X-ray powder diffraction (XRPD) data were collected on a Philips Analytical X-ray PW3710 BASED diffractometer with a Cu Kα radiation. All XRPD measurements were carried out at room temperature.

**Crystallographic Analysis.** Mo Kα radiation ($\lambda = 0.710\ 73$ Å) was used; $T = 293$ K for all compounds (SMART AXS 1000 CCD diffractometer for **1**−**5** and **8**−**10** and Philips PW1100 diffractometer for **6** and **7**). Lorentz, polarization, and absorption corrections were applied.[9] Structures solved by direct methods using SIR97[10] and refined by full-matrix least squares on all $F^2$ using SHELXL97[11] implemented in the WingX package.[12] Hydrogen atoms partly located on Fourier difference maps and refined isotropically and partly introduced in calculated positions. Anisotropic displacement parameters refined for all non-hydrogen atoms, except for compound **10**, where isotropic parameters were used. In compounds **6** and **8** a positional disorder between Cl and $CH_3$ was found. Hydrogen bonds were analyzed with SHELXL97[11] and PARST97,[13] and extensive use was made of the Cambridge Crystallographic Data Centre packages[14] for the analysis of crystal packing. Table 1 summarizes crystal data and structure determination results.

## Results and Discussion

The ligand α-(4-pyridyl)benzhydrol LOH reacts with $Pd(PhCN)_2Cl_2$, $Pd(COD)(CH_3)Cl$, and $Pd(OAc)_2$ in a 2:1 stoichiometry giving the complexes $Pd(LOH)_2Cl_2$, $Pd(LOH)_2(CH_3)Cl$, and $Pd(LOH)_2(OAc)_2$ as nonsolvate (**1**, **6**, **10**) or solvate (**2**−**5**, **7**−**9**), depending on the reaction conditions (Chart 2). The complexes $[Pd(LOH)_2Cl_2]$ (**1**) and $[Pd(LOH)_2Cl_2]\cdot 2THF$ (**5**) are obtained by direct synthesis in $CH_2Cl_2$ and in THF, respectively, while $[Pd(LOH)_2Cl_2]\cdot 2G$ (G = acetone (**2**), DMSO (**3**), and DMF (**4**)) are obtained through recrystallization of **1** from the corresponding solvent. Recrystallization from solvents with poorer hydrogen bond accepting properties (toluene, mesitylene, *p*-xylene, 1,4-dioxane, methanol, ethanol, 2-propanol, chloroform, dichloromethane, carbon tetrachloride) gives the nonsolvate **1**. The complexes were characterized through IR and $^1H$ NMR spectroscopy and single-crystal and powder X-ray diffractometry. In all the compounds the palladium has a square planar coordination with two LOH molecules, trans each other, and two anions as ligands; LOH coordinates by means of the 4-pyridyl nitrogen. The protons H4 and H5 (Chart 3) of the coordinated pyridyl rings are deshielded with respect to the free ligand ($\Delta\delta \approx 0.2$ ppm); the peak of alcoholic proton is observed only in hydrogen bond accepting solvents (DMSO, $(CH_3)_2CO$). $[Pd(LOH)_2(CH_3)Cl]\cdot 2THF$ (**7**)

(9) (a) *SAINT: SAX, Area Detector Integration*; Siemens Analytical Instruments, Inc.: Madison, WI. (b) Sheldrick, G. *SADABS: Siemens Area Detector Absorption Correction Software*; University of Goettingen: Goettingen, Germany, 1996.
(10) Altomare, A.; Burla, M. C.; Cavalli, M.; Cascarano, G.; Giacovazzo, C.; Gagliardi, A.; Moliterni, A. G.; Polidori, G.; Spagna, R. *Sir97: A new Program For Solving And Refining Crystal Structures*; Istituto di Ricerca per lo Sviluppo di Metodologie Cristallografiche CNR: Bari, Italy, 1997.
(11) Sheldrick, G. *Shelxl97. Program for Structure Refinement*; University of Goettingen: Goettingen, Germany, 1997.
(12) Farrugia, L. J. *J. Appl. Crystallogr.* **1999**, *32*, 837−838.
(13) Nardelli, M. *J. Appl. Crystallogr.* **1995**, *28*, 659.
(14) (a) Allen, F. H.; Kennard, O.; Taylor, R. *Acc. Chem. Res.* **1983**, *16*, 146−153. (b) Bruno, I. J.; Cole, J. C.; Edgington, P. R.; Kessler, M.; Macrae, C. F.; McCabe, P.; Pearson, J.; Taylor, R. *Acta Crystallogr.* **2002**, *B58*, 389−397.

**Chart 3.** Geometric Descriptors Used in the Analysis of the Molecular Conformation

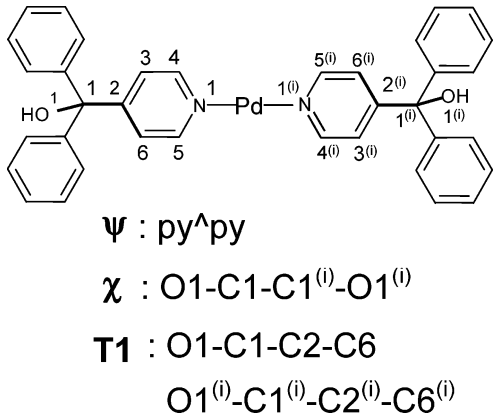


**Table 2.** Conformation of the $[Pd(LOH)_2X_2]$ Molecule in the Complexes **1**−**10**[a]

| | ψ (deg) | χ (deg) | T1 (deg) | T2 (deg) | T3 (deg) |
|---|---|---|---|---|---|
| **1** | 48.6(1) | 109.6(4) | 24.2(5) | 36.1(5) | 39.2(6) |
| | | | 30.3(6) | 32.4(6) | 39.1(6) |
| **2** | 0 | 180 | 20.4(7) | 60.1(6) | 14.2(7) |
| **3** | 0 | 180 | 20.3(2) | 65.6(2) | 14.3(3) |
| **4** | 0 | 180 | 15(1) | 69(1) | 6(1) |
| **5** | 0 | 180 | 34.5(2) | 50.5(2) | 7.4(2) |
| **6** | 45.2(2) | 109.2(6) | 29.4(9) | 32.5(9) | 39.7(9) |
| | | | 27.2(8) | 37.1(8) | 35.1(8) |
| **7** | 2.4(9) | 178(2) | −41(2) | −49(2) | −4(2) |
| | | | 27(2) | 27(2) | 9(2) |
| **8** | 0 | 180 | 30.1(3) | 58.6(3) | 5.9(3) |
| **9** | 2.3(4) | −176(1) | 42(1) | 30(1) | 32(1) |
| | | | −31(1) | −34(1) | −31(1) |
| **10** | 14.9(7) | −141(1) | 54(1) | 22(2) | 38(1) |
| | | | −26(1) | −33(2) | −51(1) |

[a] ψ = dihedral angle between pyridines; χ = reciprocal orientation of the two C−OH vectors; T1 = orientation of the C−OH vector relative to the adjacent pyridine ring; T1−T3 = conformation of the triaryl group, following Dance[15] (T1 refers to the pyridine ring and T2 to the ring involved in the *Ar*···G stacking contact).

is obtained by synthesis in THF; recrystallization from acetone gives $[Pd(LOH)_2(CH_3)Cl]\cdot 2(CH_3)_2CO$ (**8**), while recrystallization in $CHCl_3$ gives crystals of the nonsolvate $[Pd(LOH)_2(CH_3)Cl]$ (**6**) and partial decomposition of the starting complex. In the IR spectra, the most significant band is ν(OH), which follows the trend $\nu_{-OH}$(**8**) (3368 $cm^{-1}$) ≈ $\nu_{-OH}$(**2**) (3362 $cm^{-1}$) > $\nu_{-OH}$(**7**) (3289 $cm^{-1}$) ≈ $\nu_{-OH}$(**5**) (3286 $cm^{-1}$) ≈ $\nu_{-OH}$(**4**) (3279 $cm^{-1}$) > $\nu_{-OH}$(**3**) (3100 $cm^{-1}$); the sequence is in accord with the hydrogen bonds distances obtained by the structural analysis (see X-ray diffraction) and reflects the strength of the OH···G hydrogen bond. $[Pd(LOH)_2(CH_3COO)_2]\cdot$THF (**9**) was obtained by synthesis in THF, and the nonsolvate form $[Pd(LOH)_2(CH_3COO)_2]$ (**10**) by recrystallization in $CHCl_3$; however, **10** is not very stable in chlorinated solvents.

**X-ray Diffraction.** Single crystals of compounds **1**−**10** were examined by X-ray diffraction. The molecular conformation is described on the basis of the following geometric descriptors[6] (Chart 3, Table 2): the dihedral angle between pyridines (ψ); the orientation of the C−OH vectors with respect to the adjacent pyridine (T1); the reciprocal orientation of the two C−OH vectors (χ); the torsion angles $C_{ortho}-C_{ipso}-C_{sp^3}-O$ (T1, T2, T3) for each aromatic ring (labeled so that $|Ti| < 90°$, according to Dance's model for triphenylphosphines[15]). The principal interactions responsible for the crystal organization are reported in Table 3.

In **1** the $Pd(LOH)_2Cl_2$ units are assembled by −OH···Cl hydrogen bonds in chains running along *a* (Figure 1), and consequently the terminal C−OH vectors are in a gauche orientation (χ = 109°). The terminal triarylcarbinol groups can be classified as regular rotors.[15] The $Pd(LOH)_2Cl_2$ units present a $C_2$ pseudosymmetry, with the pseudo-2-fold axis passing through the palladium atom, perpendicularly to the Cl−Pd−Cl and N−Pd−N vectors, and directed along *c* (Figure 1). The molecules in the chain are related by translation; consequently, the chain pitch corresponds to *a* = 10.736(2) Å. The molecular long axes form an angle θ = 26° with *a*, the direction of propagation of the chain. The chains are associated in layers by translation along *b* in the *ab* plane (Figure 1), with Pd···Pd = *b* = 17.410(2) Å and with a minimum distance C···C = 4.3 Å between adjacent aromatic rings. The metric of these layers, defined by the bidimensional lattice *a*′, *b*′ and α′, will be the key of the discussion of the reversible solvation/desolvation processes shown by **1**. The layers have a bump-and-hollow profile, and the optimal space filling for the three-dimensional packing is achieved by 2-fold screw rotation around *b* (Figure 2). Because of the inclination of the molecular long axes relative to *a*, the adjacent, symmetry-related layers present opposite orientation of the molecules in the chains, resulting in a herringbone motif (Figure 2). The replacement of one chlorine atom in **1** with the isosteric, but hydrogen-bonding-inactive, methyl group does not result in any important modification of the crystal organization. Compound **6** is isostructural to **1**, showing that a single −OH···Cl interaction is sufficient to stabilize the chains, with the assistance of shape complementarity between complex molecules. The positions of Cl and $CH_3$ ligands can be exchanged within a chain, as shown by the disordered population of these two coordination sites in **6**. $Pd(LOH)_2Cl_2$ can host in the crystal lattice solvent molecules (G) in a 1:2 stoichiometry by generating the solvates **2**−**5**, among which **2** and **3** are isostructural, while **4** has a cell with edges and angles similar to **2** but with different unique axis and different orientation of the symmetry operations in the cell. In all cases the inclusion is based on the formation of two hydrogen bonds between the two −OH groups of the complex and the oxygen acceptor of the guest molecule G, with O···O distances ranging between 2.75 and 2.80 Å (Table 3). The resulting supramolecular $Pd(LOH)_2Cl_2\cdot 2G$ unit is invariably centrosymmetric, the molecular conformation is the same in all cases, and the positions of the G molecules coincide (Figure 3). In all cases, the complex symmetry imposes strict coplanarity to pyridines and ideal trans configuration for the terminal −OH groups. Compared to **1**, the triarylcarbinol groups show a pronounced flattening of one ring (T3 = 6−14°) and a tilting of the other (T2 = 50−69°). The $Pd(LOH)_2Cl_2\cdot 2G$ units are stacked along *a* in chains where G is sandwiched between a pair of aryl rings (*Ar*) tilted to

(15) Dance, I.; Scudder, M. *J. Chem. Soc., Dalton Trans.* **2002**, 1579.

**Table 3.** Host−Host and Host−Guest Interactions and Layer Metrics (Chain Pitch $a'$, $b'$, $\alpha'$) in the Crystal Organization of the Complexes **1**−**10** ($\theta$ = Angle That the Molecular Long Axis Forms with $a'$)

| | host−host intrachain | | | host−guest | | host−guest stacking | | layer metrics | | | |
|---|---|---|---|---|---|---|---|---|---|---|---|
| | O···Cl (Å) | O−H···Cl (deg) | | O···O (Å) | O−H···O (deg) | Ar···Ar = *a* (Å) | Ar···S (Å) | $\theta$ (deg) | *a* (Å) | *b* (Å) | $\alpha$ (deg) |
| **1** | 3.168(4) | 166(4) | | | | | | 26 | 10.7 | 17.4 | 90 |
| | 3.159(4) | 160(5) | | | | | | | | | |
| **2** | | | | 2.808(7) | 158(14) | 7.2997(9) | 3.76(1) | 57 | 7.3 | 18.6 | 90 |
| **3** | | | | 2.707(3) | 173(3) | 7.6903(3) | 3.693(3) | 57 | 7.7 | 18.5 | 90 |
| **4** | | | | 2.75(1) | 160(17) | 7.191(8) | 3.59(2) | 59 | 7.2 | 18.8 | 88 |
| **5** | | | | 2.755(2) | 171(2) | 7.9754(7) | 3.890(3) | 49 | 8.0 | 17.5 | 91 |
| **6** | 3.138(5) | 178(8) | | | | | | 25 | 10.8 | 17.4 | 90 |
| **7** | | | | 2.77(2) | 157 | 8.027(3) | 3.98(3) | 49 | 8.0 | 17.5 | 91 |
| | | | | 2.75(2) | 159 | | | | | | |
| **8** | | | | 2.865(4) | 171(4) | 7.4639(8) | 3.682(7) | 52 | 7.5 | 18.0 | 90 |
| | O···O (Å) | O−H···O (deg) | Pd···O (Å) | | | | | | | | |
| **9** | 2.77(1) | 166(4) | 3.030(6) | | | | 3.71(1) | 34 | 7.9 | 15.4 | 98 |
| | 2.79(1) | 145(4) | 3.018(7) | | | | 3.79(1) | | | | |
| **10** | 3.04(2) | 144(1) | 3.15(2) | | | | | 36 | 7.6 | 15.9 | 86 |
| | 2.47(3) | 162(1) | 3.06(2) | | | | | | | | |

larger torsion angles (T2) (compound **2,** Figure 4); the stackingdistances *Ar*···G range between 3.59 and 3.89 Å (Table 3), while the stacking pitches *Ar*···*Ar* coincide with the *a* axes of the cells. The molecular long axes are tilted relative to the chain direction ($\theta$ = 49−59°). Chains are translated by similar steps along *b* for **2** and **3** ($b' = b$), along the *b*−*c* cell diagonal for **5** ($b'$ = 17.507 Å) and along *c* for **4** ($b' = c$), thus originating layers with the same metrics (average $a'$ = 7.6 and $b'$ = 18.1 Å; $\alpha'$ = 90°). This arrangement creates channels along *a* with alternating aromatic rings allocating solvent molecules between. Solvates **2**−**5** are differentiated by the mode of association of the identical layers in the third direction (Figure 5). In **2** and **3** adjacent layers are generated by a screw $2_1$ rotation around *b*, while in **5** they are related by simple translation along the $b + c$ diagonal and in **4** by a *c* glide plane. The main consequence of these different arrangements regards the orientation of the molecular axes in chains of adjacent layers: a herringbone motif results for **2** and **3**, similar to the one observed in **1**, while parallel rows appear in **4** and **5**. The effects of the substitution of one Cl atom with a $CH_3$ group have been tested also for **2** and **5**. The methylated THF solvate **7** is isostructural with the dichloro analogue **5**, while, unexpectedly, the methylated acetone solvate **8** is not arranged in the herringbone pattern found in **2** but it is isostructural with **7** and **5** (Figure 5), with slight modifications of the cell but retention of the layer metrics (Table 3). Substantially, the Cl/$CH_3$ exchange does not have any effect on the crystal organization (isostructurality of **1** with **6** and of **5** with **7**). The alternation of the solvate layers can proceed both in the herringbone (**2**, **3**) and in the parallel (**4**, **5**, **7**, **8**) arrangements, and this suggests the possibility of herringbone/parallel packing polymorphs for each solvate.

The robustness, relative to a change in size and accepting character of the anion, of the chain motif observed in **1** and **6** was verified by analyzing the crystal arrangement of $Pd(LOH)_2(CH_3COO)_2$ (**10**); its solvation properties were examined in the THF monosolvate form **9**. As regards molecular conformation (Table 2), compound **10** is midway between the centrosymmetric complex found in **2**−**5** and the pseudo-$C_2$ conformation typical of **1** and **6**. Similarities to

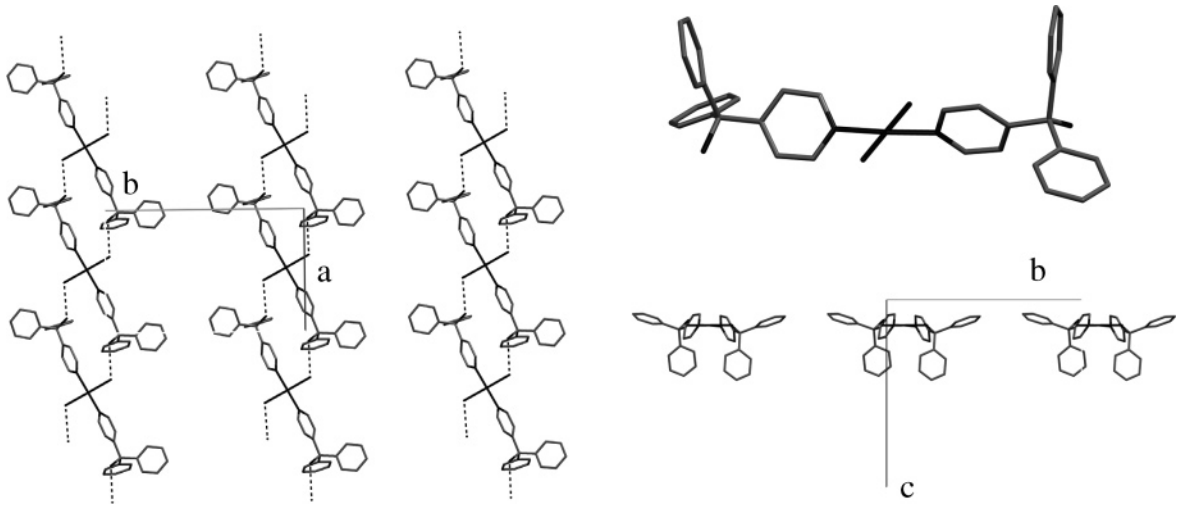


**Figure 1.** Organization of one molecular layer in the crystal structure of **1** (left) with OH···Cl hydrogen bonds dashed and hydrogen atoms omitted, edge-on view of the layer (right bottom), and molecular conformation (right top) of $Pd(LOH)_2Cl_2$ in **1**.

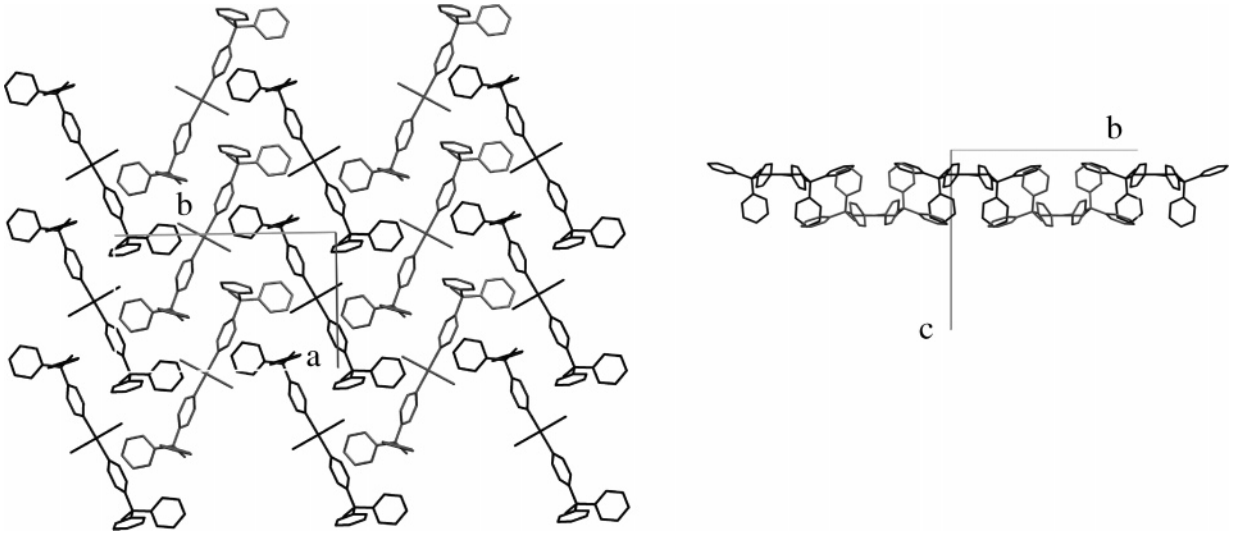


**Figure 2.** Herringbone arrangement of two consecutive layers in **1** (left) and edge-on view of the packing of two complementary layers, obtained by 2-fold screw rotation around *b* (right). Different layers are represented by different shades of gray.

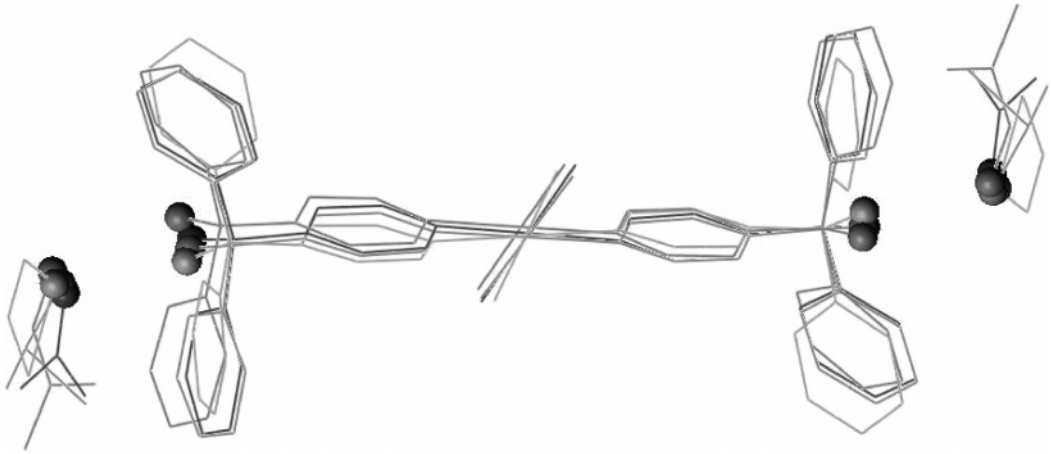

**Figure 3.** Superimposition of supramolecular $Pd(LOH)_2Cl_2.2S$ units for **2**−**5**. Hydrogen bond donors and acceptors are evidenced as balls.

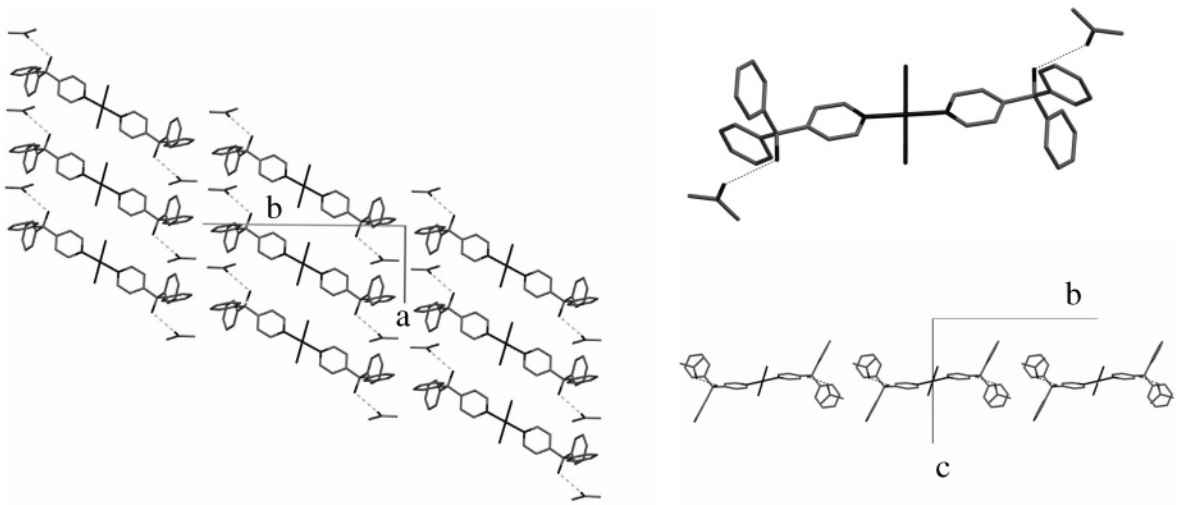


**Figure 4.** Organization of one molecular layer in the crystal structure of **2** (left) with OH···O(acetone) hydrogen bonds dashed and hydrogen atoms omitted, edge-on view of the layer (right bottom), and molecular conformation (right top) of $Pd(LOH)_2Cl_2{\cdot}2(CH_3)_2CO$ in **2**. Compound **3** is isostructural to **2**. The layer arrangements for **4**, **5**, **7**, and **8** are similar.

the nonsolvate prototype include rotor conformation of terminal triaryl groups and $\chi$ different from 180°; analogies to solvate forms regard pyridines almost coplanar, opposite torsion angles for terminal triaryl groups, and −OH groups pointing toward trans configuration. The overall organization of the $Pd(LOH)_2(CH_3COO)_2$ units in **10** is similar to **1**, with association in chains where the $-OH\cdots O(CO)CH_3$ hydrogen bonds replace the −OH···Cl interactions (Figure 6). Com-

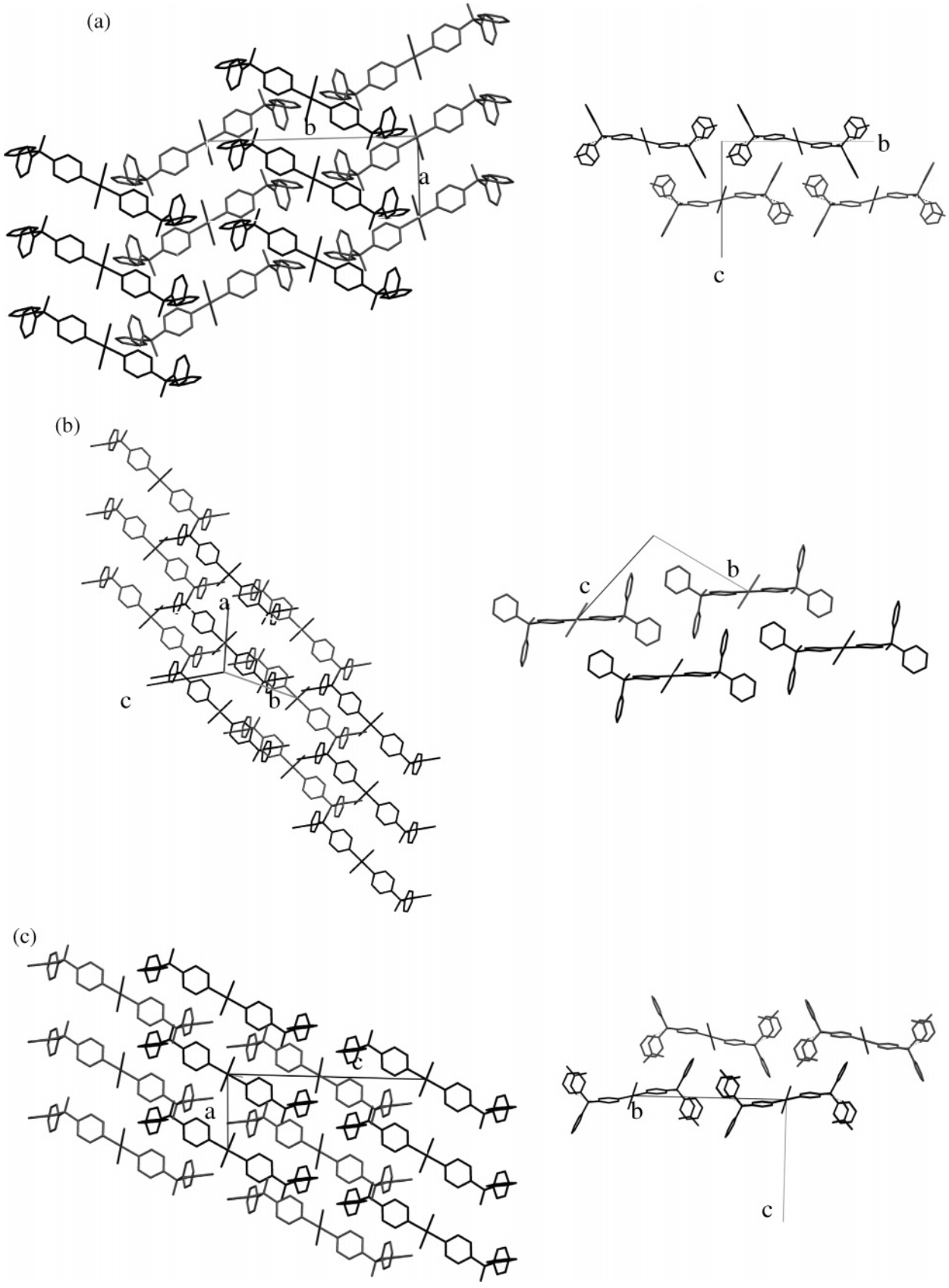


**Figure 5.** Arrangement of consecutive layers in solvates **2**−**5** with layers differentiated by shades of gray (solvent molecules omitted): (a) herringbone pattern for **3** and **2** (left) and edge-on view (right), showing the $2_1$ relation between layers; (b) parallel pattern for **5** (left) and edge-on view (right), showing that layers are related by translation; (c) parallel pattern for **4** (left) and edge-on view (right), showing that layers are related by a *c* glide perpendicular to *b*.

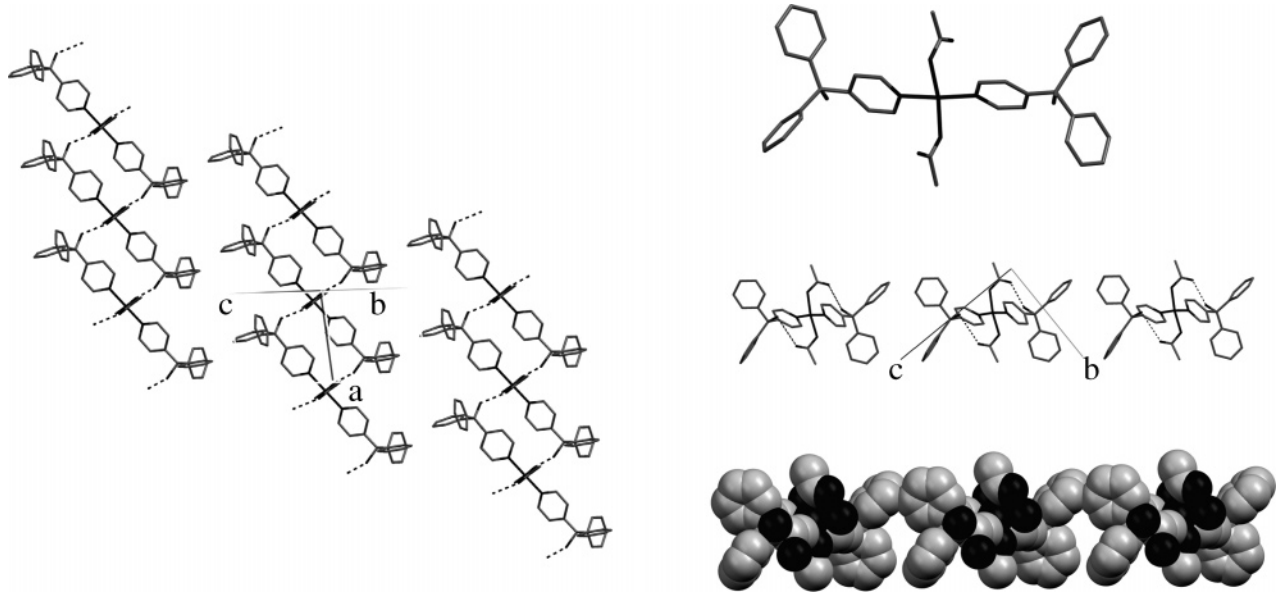


**Figure 6.** Organization of one molecular layer in the crystal structure of **10** (left) with OH···O(acetate) hydrogen bonds dashed and hydrogen atoms omitted and molecular conformation of $Pd(LOH)_2(CH_3COO)_2$ in **10** (right top) with edge-on views of the layer, in stick and space-filling views, showing the presence of voids between aromatic rings (right bottom).

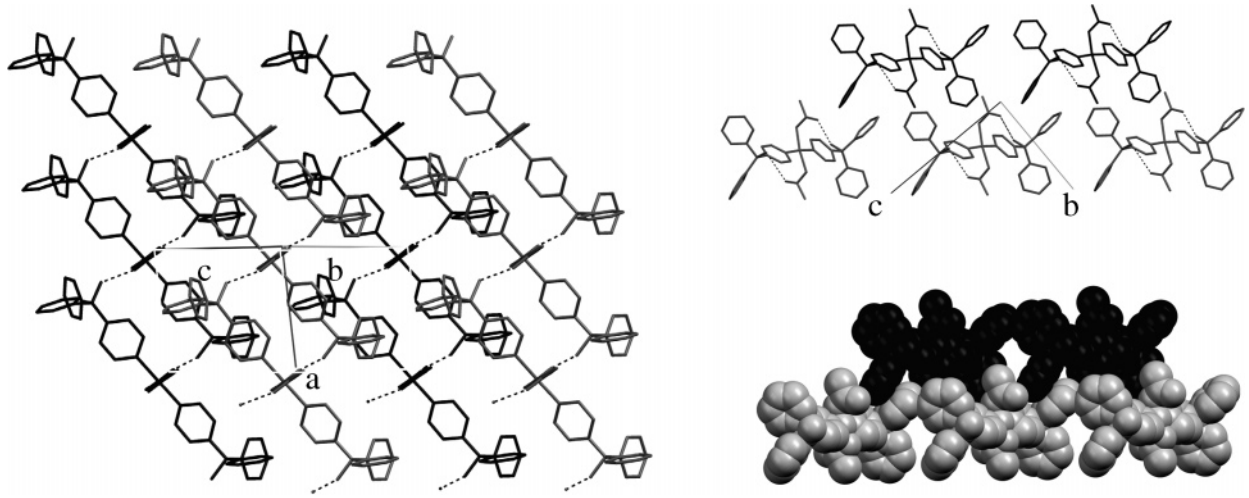


**Figure 7.** Parallel arrangement of two consecutive layers in **10** (left) with edge-on views in stick and space-filling renderings of the packing of two adjacent layers, related by translation (right). Different layers are represented by different shades of gray.

pared to the chloride, the acetate ligand allows the formation of shorter hydrogen bonds (Table 3) and the chains are stabilized by additional O(H)···Pd contacts. The chains run along *a* and are assembled in layers along the *b*−*c* cell diagonal whose metric ($a' = 7.57$ and $b' = 15.86$ Å; $\theta = 36°$) is similar to the one observed for the solvate forms, while the molecular orientation within the chains is intermediate between the nonsolvate and the solvate forms. Moreover, the unit cell of compound **10** is comparable with those of **3** and **8**, even with some angular distortions (Table 1). Interestingly, in **10** the assembly of the layers occurs by translation (Figure 7), giving the parallel pattern observed in precedence only for the solvate forms. This arrangement leaves some space between the chains within the layers (Figure 7). The uptake of one THF molecule by **10** gives **9**, Figure 8, which could be an intriguing picture of the first step of the mechanism converting the nonsolvate into the solvate forms. **9** is quasi-isostructural with **10** (Table 1); there is no host−guest hydrogen bonding, but THF is clathrated in the channels running along *a*. Clathration is assisted by interchain stacking of THF between two parallel aromatic rings belonging to adjacent chains, with distances comparable to the ones typical of the intrachain stacking of disolvates. As in **10**, chains are formed by OH···O(acetate) short hydrogen bonds and weak O···Pd contacts (Table 3). The chain inclination relative to *a* ($\theta = 34°$) and the layer metrics ($a' = 7.930$ and $b' = 15.409$ Å; $\alpha' = 98°$) are similar to **10**. The layers are assembled by translation in the parallel pattern. On the other hand, the molecular conformation tends to the one observed for solvates: even if the monosolvation imposes the *P*1 space group, the $Pd(LOH)_2(CH_3COO)_2$ molecule is nearly centrosymmetric (Table 2), and in particular pyridines are coplanar and −OH groups are trans each other. The regular rotor conformation of the triaryl groups is related to the absence of intrachain stacking interactions involving the guest.

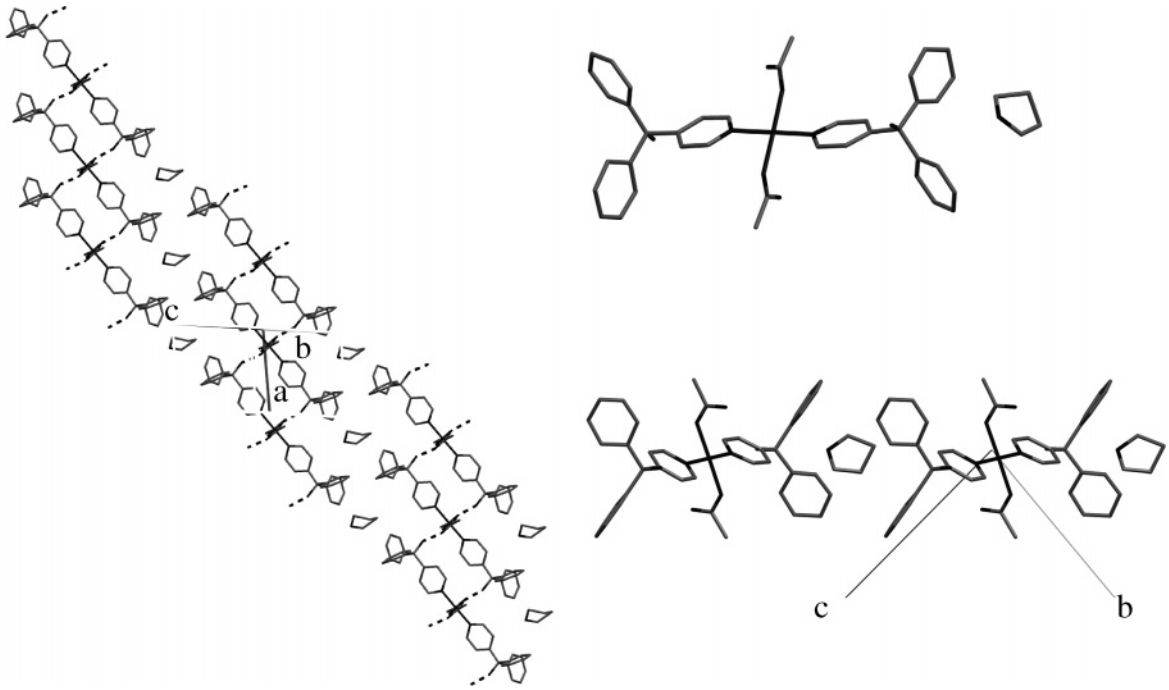


**Figure 8.** Organization of one molecular layer in the crystal structure of **9** (left) with OH···O(acetate) hydrogen bonds dashed and hydrogen atoms omitted, edge-on view of the layer evidencing clathration of guest (right bottom), and molecular conformation of $Pd(LOH)_2(CH_3COO)_2 \cdot THF$ in **9** (right top).

The comparison of of the whole set of compounds **1**−**10** provides the structural framework which must be taken into account for the formulation of a mechanicistic model for the solvation/desolvation process. The observed structures represent still pictures of the steps of the process; we propose a way to link those steps by the simplest geometric rearrangements required to convert from one structure to the other. All the structures are organized according to the highly conserved motif represented by the layer of molecules built by translation on a bidimensional lattice with average values $a' = 7.6$ Å, $b' = 18.1$ Å, and $\alpha' = 90°$ for the solvate (**2**−**5**, **7**−**9**) and $a' = 10.7$ Å, $b' = 17.4$ Å, and $\alpha' = 90°$ for the nonsolvate forms (**1**, **6**, **10**). In the solvate structures, the guest molecules are included by host−guest hydrogen-bonding and stacking interactions in the space between the chains within the layer; the host molecules form an angle of $\theta = 54°$ with the $a'$ axis of the mesh. In the nonsolvate structures, the molecules interact by OH···Cl hydrogen bonds with $\theta = 26°$. The release of guest molecules during desolvation triggers a rotation in $\theta$ by 28° of all the molecules in the plane, with a slight adjustment of the mesh dimensions (Scheme 1). The breaking of host−guest and the concomitant formation of host−host hydrogen bonds also implies a conformational rearrangement, with conversion of $\chi$ from trans to gauche and of the triaryl groups geometry from flattened to regular rotor conformation. The reversibility of the desolvation/solvation process is possible because of the minimum displacements required for the single host molecules and by the modest reorientation necessary for their molecular long axes. This mechanism accounts for the conversion **2**−**3** ⇔ **1**, where the propagation of chain rotation in symmetry-related adjacent layers of **2**−**3** produces the correct herringbone pattern found in **1**. To convert the solvate forms **4**, **5**, **7**, and **8,** characterized by the parallel arrangement

**Scheme 1.** Desolvation and Solvation Mechanism[a]

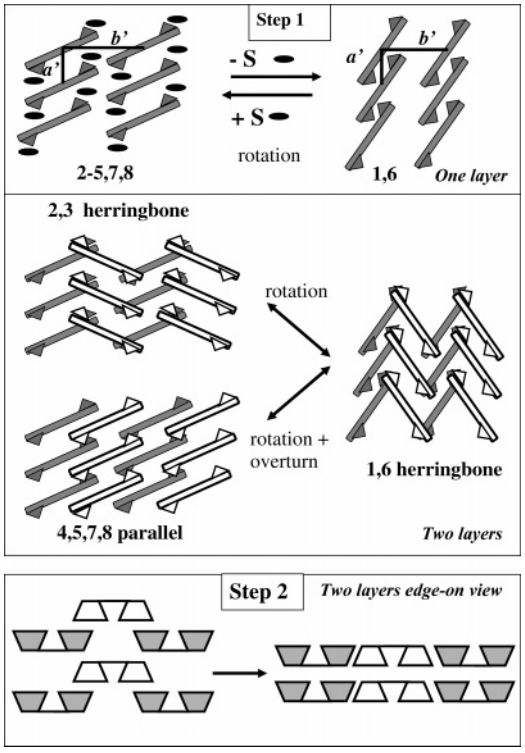


[a] Thick bar = complex; triangle = terminal OH.

of adjacent layers, into the herringbone nonsolvate **1** and **6** forms, the simultaneous intralayer rotation must be accompanied by an overturning of alternate layers, achievable by tilting of each molecule around the $b'$ axis. The structural correlations between solvate and nonsolvate structures in these complexes recall the concept of "structural filiation", proposed to describe dehydration and other solid−solid transformations of dihydrated copper(II) 8-hydroxyquinoli-

nates.[16] According to this model, the desolvation mechanism described in this paper can be tentatively classified as a cooperative reorganization with transmission of structural information: in both the herringbone and the parallel cases, the rotation and rotation/overturn mechanisms (filiation step 1) lead to a nonsolvate material which is the precursor of the stable crystalline form **1**, finally obtained by sliding adjacent layers to compact the packing (filiation step 2) (Scheme 1).

On the other hand, insights regarding the solvation process may be found by analyzing the relations among the acetate complexes **10** and **9** and their **1** and **5** chloride counterparts. While the apohost **1** needs to rearrange its building blocks to accommodate the guest and give the solvate forms,[17] in **10** the intralayer packing of the chains is looser than in **1,** due to the slightly larger $\theta$ and to the layer metrics ($a' =$ 7.9 Å, $b' = 15.9$ Å, $\alpha' = 86°$) similar to **5**. In this sense, **10** is fitter to accommodate a guest, which in fact is included by clathration in **9**, without significantly disrupting the layer network. **9** depicts the first event of the structural rearrangement accompanying the solvation process, showing the incipient uptake of one THF molecule between the chains; the −OH groups may be directed to hook the guest and stack it between two rings, converting to the situation in Figure 4. The higher stability of the hydrogen-bonded chains involving the acetate accounts for the difficulty of proceeding further in the solvation process for **9**, as the inclusion of the second guest molecule would require the breaking of the O−H···O and Pd···O intrachain interactions. Moreover, the parallel arrangement of layers in **10** points to the possible existence of supramolecular isomers also for the nonsolvate forms **1** and **6**.

**Thermal Analysis and Solvation/Desolvation Experiments.** The thermal stability of **2** (herringbone packing), **4** (parallel packing), and **9** (clathrate monosolvate) was tested by thermogravimetric analysis (TGA) and differential scanning calorimetry (DSC). TGA scans revealed that **2** releases both the acetone guests in a single narrow step (80−115 °C), and similarly **4** loses both DMF molecules simultaneously between 110 and 160 °C. On the other hand, compound **9** releases the single THF molecule on a broad temperature range (80−160 °C), as a consequence of the much less specific host−guest interactions found in this compound compared with **2** and **4**. DSC measurements show endotherm peaks in correspondence with the desolvation events; however, the DSC trace of **2** evidences also an exothermic phenomenon which persists upon variation of the scan speed, under the endothermic process. This could be related to the molecular reorientation among and within the layers with formation of new hydrogen bonds that is concomitant to the leaving of the guest, during the conversion of **2** into the apohost **1**. The related process for **4** could be hidden by the desolvation endotherm. Scheme 2 summarizes the results of the DSC experiments for **2**, **4**, and **9**.

The capability of the apohosts **1** and **10** to uptake solvent vapors to convert into **2**, **4**, or **9** with reversible processes has been demonstrated by performing the desolvation/solvation cycles shown in Scheme 3. At every stage, the identity of the products was confirmed by infrared spectroscopy and X-ray powder diffraction. **1** transforms into the acetone (**2**) or DMF (**4**) solvate both by recrystallization from the guest solvent and by solid-state inclusion; **1** does not include vapors of THF. The process is reversible: by heating under vacuum, **2** and **4** lose solvent and give the apohost **1**. The crystalline powders of **1** obtained in this way are identical with the product of the direct synthesis, and they include vapors of acetone to give microcrystalline powder of **2**.

**Scheme 2.** Results of the DSC Experiments for **2**, **4**, and **9**

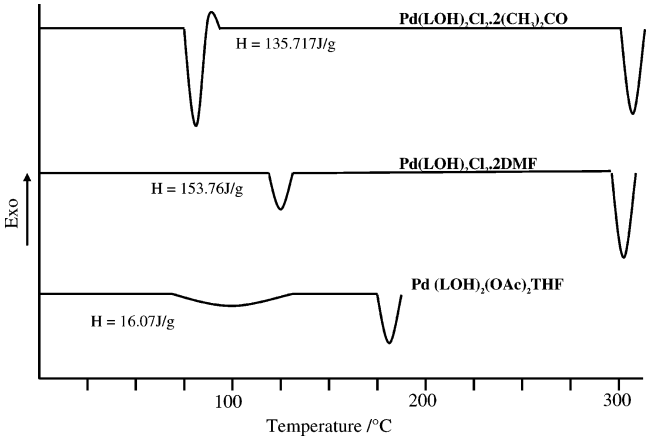


**Scheme 3.** Solvation/Desolvation Experiments

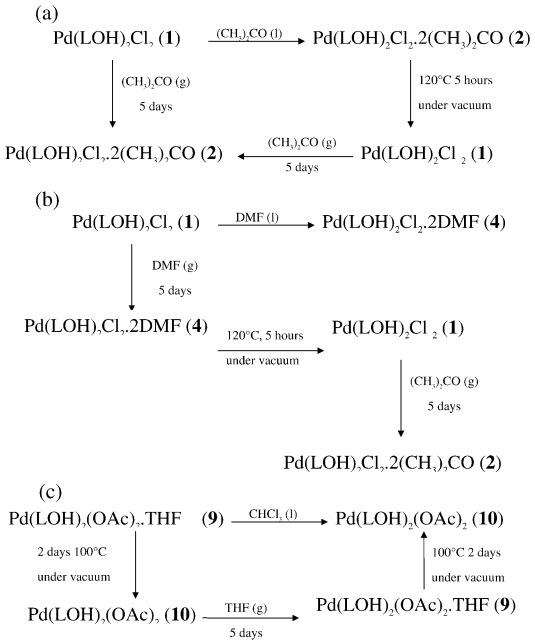


## Conclusions

$Pd(LOH)_2Cl_2$ represents a novel type of organic−inorganic wheel-and-axle diol with good inclusion properties. Its crystal form **1** hosts several hydrogen bond accepting solvents, either via dissolution/ricrystallization or via gas/solid absorption, giving crystalline solvates with $Pd(LOH)_2Cl_2 \cdot 2G$ stoichiometry. The crystalline nonsolvated apohost **1** is recovered by

(16) Petit, S.; Coquerel, G. *Chem. Mater*. **1996**, *8*, 2247−2258.
(17) Nassimbeni, L. R. *Acc. Chem. Res.* **2003**, *36*, 631−637.

guest removal upon heating under vacuum. On the basis of structural evidence, a path describing the rearrangements required to convert between the solvated and unsolvated compounds implying modest structural alterations has been formulated. The structural analysis shows that the apohost is preorganized for inclusion and that solvent uptake/release involves a "venetian blinds" mechanism based on concerted oscillations of the complex molecules around the palladium atoms. These molecules are organized in layers with practically invariant metrics, and the oscillation occurs with slight conformational rearrangements, implying $\bar{1} \Leftrightarrow C_2$ conversion in the molecular symmetry. The solvate layers assemble in two isomeric forms: with parallel or herringbone orientation of the molecules between different layers. A further long-range rearrangement, along with intralayer reorientation, is required to convert between parallel and herringbone patterns. As suggested by the analysis of $Pd(LOH)_2(CH_3COO)_2$, the first step of the solvent uptake could be the insertion of one guest molecule in the space between the chains within a layer. This would trigger the molecular reorientation necessary to realize the host−guest hydrogen-bonding and stacking interactions, thus leaving space for the incoming of the second solvation molecule. Variable-temperature X-ray powder diffraction experiments and accurate coupled DSC/TGA measurements are planned to clarify the nature of the desolvation process and to inspect for possible polymorphism of these systems.

**Acknowledgment.** We thank the "Centro Interfacoltà Misure Giuseppe Casnati" and the "Laboratorio di Strutturistica Diffrattometrica" of the University of Parma.

**Supporting Information Available:** CIF data, including final atomic coordinates with esd's for all non-H atoms, calculated coordinates for all atoms introduced in idealized positions, anisotropic thermal parameters, and a full list of bond distances and angles for **1**−**10**, perspective views of compounds **1**−**10**, thermal analysis (TGA and DSC) traces, and X-ray powder diffraction characterization of compounds involved in the solvation/desolvation experiments. This material is available free of charge via the Internet at http://pubs.acs.org.

IC048896M